American Mineralogist, Volume 84, pages 333–340, 1999

Compressibility mechanisms of alkali feldspars: New data from reedmergnerite

R.T. Downs,* H. Yang, R.M. Hazen, L.W. Finger, and C.T. Prewitt

Geophysical Laboratory, Carnegie Institution of Washington, 5251 Broad Branch Road, N.W., Washington, D.C. 20015, U.S.A.

Abstract

Structural and volume compressibility data for reedmergnerite, $NaBSi_3O_8$, were obtained by single-crystal X-ray diffraction at pressures up to 4.7 GPa. The bulk modulus was determined to be 69.8(5) GPa with the pressure derivative constrained to 4. Unit-cell compression is anisotropic, as indicated by unit strain tensors. Tetrahedral bond lengths and angles remained relatively constant over the pressure interval, whereas Na-O bonds decreased systematically. T-O-T angles underwent a variety of behaviors, remaining constant or decreasing with pressure.

The compression for reedmergnerite is similar to that of low-albite, wherein bending of the (Al,B)-Oco-Si angle compresses the Na-bearing zigzag channels. In contrast, microcline compresses by shearing the four-membered rings, which in turn compresses the K-bearing channels. At about 4 GPa, a new bond between K and Obm appears that alters the compression mechanism and explains the discontinuity in the pressure variation of crystallographic parameters observed by Allan and Angel (1997). Thus, the compression mechanism of the alkali feldspars is dominated by the compression of alkali containing channels. However, because of low symmetry, this can be accomplished in several ways. The observed variety of compression pathways resulted from T-O-T angle bending energetics that were coupled with the effects of alkali cation bonding.

Introduction

Feldspars are crustal materials and therefore not naturally subjected to high pressure. However, considerable interest exists in the response of the feldspar structure to pressure. For example, such low-density structures exhibit both subtle and extreme structural changes when subjected to only modest pressures and, furthermore, the low symmetry of ordered feldspars maximizes the degrees of freedom associated with compression mechanisms.

Compression mechanisms are structurally controlled. Whereas highly symmetric closest-packed deep earth materials compress mainly by bond shortening, shallow earth materials mainly compress by bond angle bending. For example, Si-O-Si angle bending correlates with the compressibility of the SiO_2 polymorphs (Hemley et al. 1994). They all seem to fall on the same $\Delta V - \Delta$(Si-O-Si) trend (Downs and Palmer 1994). The compressibility of an individual silica structure is simply related to the displacements of the $<$Si-O-Si$>_O$ angles from their global equilibrium value ($\sim$144°); the further from equilibrium, the stiffer the structure. However, the feldspars are not as simple. The T-O-T angle differs from being only Si-O-Si, as in silica, to being a mix of, for instance, Si-O-Si and Al-O-Si (or B-O-Si). These angles have significantly different curvatures in their variations with energy. Al-O-Si appears to be twice as soft as Si-O-Si, whereas B-O-Si is twice as stiff (Nicholas et al. 1992). If compressibility of feldspars was dependent only upon these factors, then albite, potassium feldspar, and anorthite should be softer than the low-density silica polymorphs because the Al-O-Si angle is weaker than the Si-O-Si angle. Instead, the feldspars are generally stiffer; bulk moduli for quartz, cristobalite, and the high-pressure polymorph, coesite, are 37, 11, and 100 GPa, respectively (Angel et al. 1997; Hemley et al. 1994) but equal 55, 60, 80, and 69 GPa for albite, microcline, anorthite, and reedmergnerite, respectively (Angel 1994). Thus, the M-cation must effect compressibility, even though compression proceeds through T-O-T angle bending.

The M-cation affects the bending energy of the T-O-T angle primarily through the charge of the M-cation and the M-O bond length. Also, the energy required for the bending of a T-O-T angle is significantly increased if the bridging O is bonded to three or more atoms (Geisinger et al. 1985). An atom with more electrons to contribute to bonding will produce a stronger bond than another atom with fewer electrons at the same bond length, and as the bond lengthens, the electron density becomes more diffuse and, therefore, the contribution to the bonding energy is lower. These effects are demonstrated by comparing the compressibility of anorthite (Angel 1994) containing Ca with feldspars containing Na or K. If compression were controlled only by the T-O-T angles, then anorthite, with every bridging angle between Al and Si, should be more compressible than sodium or potas-

* Present address: Department of Geosciences, University of Arizona, Tucson, Arizona 95721-0077, U.S.A. E-mail: Downs@geo.arizona.edu

0003–004X/99/0003–0333$05.00

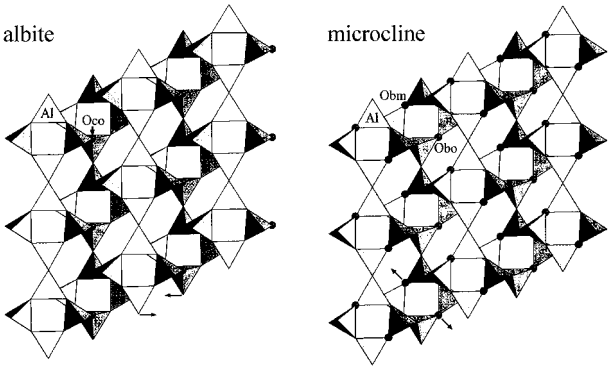

FIGURE 1. The structure of albite and microcline viewed down b^* with $0.0 < y < 0.5$. Differences in compression mechanism between the two structures are illustrated. The T-Oco-T angle in albite bends in such a way that the chains effectively slide over each other as demonstrated by the arrows in the bottom of the figure. In microcline the major angle bending occurs at Obo and Obm, effectively shearing the four-membered rings as again demonstrated with the arrows at the bottom of the figure.

sium feldspars, where half the bridging angles are between Si atoms only. However, sodium and potassium feldspars are more compressible than anorthite. This is due to the effect of electrons from a closer, more highly charged Ca atom on the bridging bond.

Surprisingly, however, potassium feldspars are less compressible than sodium feldspars. From Bridgman (1923) type molar volume–compressibility arguments it would be expected that sodium feldspars would be more incompressible than potassium feldspars because the Na-O bond is shorter than the K-O bond, and the molar volume of the sodium feldspars is smaller. This demonstrates that it is not sufficient to consider only the average length of the M-O bond. Electron density maps show that K is sevenfold coordinated, whereas Na is fivefold (Downs et al. 1996). The most compressible direction in low albite is that which decreases the width of the channels containing the alkali cation (Downs et al. 1994). The variation of the T-O-T angles defines the details of the compression pathway. In particular, the Oco atom in albite was not bonded to Na. This means that Oco in albite is underbonded in an Al-Oco-Si linkage that would be quite soft compared to any other angle in the structure. The bending of this angle directly aids compression of the alkali-containing channel by letting the chains of four-membered rings slide over each other (Fig. 1). The structure work on albite shows that the Al-Oco-Si angle is indeed the most compressible angle in the structure. Furthermore, in line with the observation that Al-O-Si angles are weaker than Si-O-Si angles, only Al-O-Si angles decreased with pressure. The Si-O-Si angles remain constant or even show an increase.

Allan and Angel (1997) found that the compression mechanism in microcline is quite different from that in albite. The Al-Oco-Si angle undergoes the least change with pressure in microcline, whereas in albite it changes the most. The electron density study showed that Oco was bonded to K in microcline, so its bending force constant should be effectively increased. In microcline, the Al-Obo-Si and Si-Obm-Si angles display the greatest decreases with pressure. This corresponds to a shearing of the four-membered rings (Fig. 1). The net effect still decreases the width of the channel.

Substitution of different tetrahedral cations also affects the compressibility of the feldspar structure. Hackwell and Angel (1992) undertook a powder XRD study of cell parameters for albite, reedmergnerite, anorthite, and danburite ($CaB_2Si_2O_8$) and showed that the B analogue is more incompressible than the Al containing structure. In albite and reedmergnerite, the <T-O-T> angles are similar and there is only 0.07 Å difference in <R(Na-O)> (Hackwell and Angel 1992). Therefore, the differences in compressibility must be due to the differences in bending force constants of B-O-Si vs. Al-O-Si. This paper examines in detail the influences of the M cation on the T-O-T linkages, along with the effect of the composition of the T cation by studying and comparing the compression mechanisms of reedmergnerite, $NaBSi_3O_8$, with that in low-albite ($NaAlSi_3O_8$) and microcline ($KAlSi_3O_8$).

EXPERIMENTAL METHODS

Structure refinement at room pressure

Reedmergnerite (N.M.N.H. 140710) from the Joseph Smith no. 1 mine, Duchesne County, Utah, was kindly provided by Paul Powhat of the Smithsonian Institution. This type locality is described by Milton et al. (1954, 1960). Samples from the same locality were studied by Appleman and Clark (1965). Fleet (1992) and Hackwell and Angel (1992) used a crystal from the same specimen as ours. In natural samples it is found that the B atom is highly ordered into the T1o site (Fleet 1992). However, the tetrahedral site ordering sequences obtained from high-temperature synthetic samples are very unusual compared to albite, but they do seem to correlate with stereochemical features. These previous studies indicate that our sample is pure $NaBSi_3O_8$ with B fully ordered into the T1o site.

A (001) cleavage fragment measuring approximately $100 \times 70 \times 50$ m was chosen. Room-pressure diffraction data were collected in air on an automated Huber four-circle diffractometer operated at 45 kV and 40 mA using monochromatic Mo$K\alpha$ radiation ($\lambda = 0.7093$ Å). Each reflection profile was examined to verify crystal perfection and that twinning was not present. The symmetry of the crystal was confirmed to be $C\bar{1}$, with cell dimensions (Table 1) obtained from refining the positions of 31 reflections of high intensities between 10° and 32° 2θ.

A hemisphere ($l > 0$) of intensity data was collected to $\sin\theta/\lambda = 0.7$ Å^{-1} (or $2\theta = 60°$) from a total of 1655 symmetrically distinct reflections. No absorption correction was applied to the intensities because of the sufficiently small value of the linear-absorption coefficient ($\mu_L = 8.66$ cm^{-1}). Neutral atomic scattering factors (Doyle

TABLE 1. Reedmergnerite unit-cell data as a function of pressure

P (GPa)	*a* (Å)	*b* (Å)	*c* (Å)	α (°)	β (°)	γ (°)	*V* (Å³)
0.00*	7.8386(3)	12.3733(5)	6.8074(3)	93.319(3)	116.368(3)	92.040(3)	589.18(4)
0.00†	7.8383(6)	12.3720(4)	6.8073(7)	93.317(6)	116.357(6)	92.039(5)	589.14(7)
0.00(5)*	7.8389(7)	12.3715(6)	6.8065(12)	93.311(9)	116.363(8)	92.043(6)	589.06(11)
0.58(5)	7.8022(13)	12.3517(10)	6.7969(16)	93.325(15)	116.358(14)	92.080(11)	584.53(16)
0.88(5)*	7.7852(10)	12.3419(5)	6.7917(9)	93.332(7)	116.347(10)	92.094(6)	582.37(9)
1.89(5)*	7.7231(9)	12.3038(5)	6.7719(12)	93.364(9)	116.316(10)	92.145(6)	574.36(12)
2.47(5)	7.6862(10)	12.2833(8)	6.7600(7)	93.372(13)	116.284(10)	92.187(9)	569.78(9)
3.00(7)*	7.6589(10)	12.2675(6)	6.7512(7)	93.374(10)	116.256(10)	92.222(8)	566.40(9)
3.36(6)	7.6366(10)	12.2561(5)	6.7445(8)	93.380(8)	116.231(10)	92.249(6)	563.75(9)
3.64(7)*	7.6194(9)	12.2465(6)	6.7389(18)	93.392(10)	116.222(11)	92.263(7)	561.60(16)
4.21(5)	7.5923(9)	12.2306(6)	6.7294(8)	93.374(10)	116.191(9)	92.300(8)	558.22(9)
4.68(9)*	7.5790(7)	12.2200(6)	6.7141(7)	93.373(10)	116.303(8)	92.345(7)	554.92(8)

Notes: Space group symmetry is $C\bar{1}$.
* Intensity data collected at these pressures.
† Sample in the diamond anvil cell with no pressure medium and no applied pressure to check that the orientation of the crystal provided sufficient access to reciprocal space.
‡ Obtained under pressure that was sufficient to remove the air bubble.

and Turner 1968), as well as real and imaginary anomalous dispersion corrections, were used to model the electron distribution. We refined the structure with anisotropic displacement factors and type 2 isotropic extinction (Becker and Coppens 1975) to $R = 0.024$ and $R_w = 0.027$ using a revised version of RFINE4 (Finger and Prince 1975). The structure factors were weighted by $[\sigma_F^2 + (pF)^2]^{-1}$, where σ_F was obtained from counting statistics and $p = 0.021$ was chosen to ensure that the errors were normally distributed through probability plot analysis (Ibers and Hamilton 1974). The goodness of fit is 1.12. The refined values of the positional and displacement parameters (Table 2) are in excellent agreement with the data of Fleet (1992), justifying the assumption of a pure sample with complete order.

High-pressure lattice parameters

The crystal was mounted into a miniature 3-pin diamond anvil cell (modified after Merrill and Bassett 1974) with a 4:1 methanol to ethanol mixture as a pressure medium. The pressure calibration was facilitated by fitting Lorentzian functions to the fluorescence spectra of several small ruby chips that were included in the cell. We determined the pressure from least-squares estimates of the positions of the R_1 and R_2 lines using the relationship established by Mao et al. (1978) with an error of approximately 0.05 GPa. The positions of 16 reflections between 17° and 30° 2θ were determined with the eight-reflection centering technique (King and Finger 1979) at 11 different pressures up to 4.68(9) GPa. Least-squares refinement of the diffraction data gave the cell dimensions reported in Table 1.

Structure refinements at high pressures

Intensity data for the reedmergnerite crystal were recorded up to $\sin\theta/\lambda = 0.7$ Å^{-1} for refinements of the structure at 0.00, 0.88, 1.89, 3.00, 3.64, and 4.68 GPa on the Huber diffractometer. We used ω scans of 1° widths in steps of 0.025° and counting times of 10 s per step. At each pressure we examined peaks that violate $C\bar{1}$ symmetry but none were found that had significant intensity. The intensity data were corrected for the effects of diamond cell absorption, as well as other standard procedures, and structural parameters were refined with RFINE4 as described in the room pressure section of this paper. A summary of the refinement statistics as well as

TABLE 2. Reedmergnerite structural data at room conditions

Atom	*x*	*y*	*z*	B_{eq}	β_{11}	β_{22}	β_{33}	β_{12}	β_{13}	β_{23}
Na	0.25820(9)	0.00757(5)	0.1330(1)	1.63(1)	0.0050(1)	0.00324(5)	0.0110(2)	0.00034(5)	0.0024(1)	−0.00228(7)
B	0.0121(2)	0.1617(1)	0.2216(2)	0.53(2)	0.0027(2)	0.00076(7)	0.0039(3)	−0.0001(1)	0.0013(2)	0.0000(1)
Si1m	0.00585(5)	0.80964(3)	0.20972(6)	0.473(8)	0.00250(7)	0.00072(2)	0.0033(1)	0.00027(3)	0.00120(6)	0.00017(3)
Si2o	0.70279(5)	0.10181(3)	0.32049(6)	0.496(8)	0.00237(7)	0.00060(2)	0.0041(1)	0.00000(3)	0.00114(6)	0.00002(3)
Si2m	0.68488(5)	0.86453(3)	0.35447(6)	0.479(8)	0.00240(7)	0.00064(2)	0.0037(1)	0.00018(3)	0.00119(6)	0.00018(3)
Oa1	0.0078(1)	0.13652(8)	0.0041(2)	0.79(2)	0.0052(2)	0.00113(5)	0.0046(2)	0.00021(7)	0.0023(2)	0.00020(9)
Oa2	0.5933(1)	0.98123(7)	0.2758(2)	0.66(2)	0.0028(2)	0.00066(5)	0.0060(3)	0.00009(7)	0.0011(2)	0.00037(8)
Obo	0.8449(1)	0.09894(8)	0.2112(2)	0.93(2)	0.0049(2)	0.00121(5)	0.0087(3)	−0.00073(8)	0.0043(2)	−0.00054(9)
Obm	0.8163(1)	0.83485(8)	0.2335(2)	0.95(2)	0.0043(2)	0.00168(6)	0.0080(3)	0.00056(8)	0.0036(2)	0.0003(1)
Oco	0.0066(1)	0.27645(8)	0.2736(2)	0.80(2)	0.0038(2)	0.00086(5)	0.0080(3)	0.00016(7)	0.0030(2)	−0.00019(9)
Ocm	0.0287(1)	0.67957(8)	0.2062(2)	0.82(2)	0.0040(2)	0.00092(5)	0.0063(3)	0.00063(7)	0.0012(2)	0.00021(9)
Odo	0.1903(1)	0.11840(8)	0.3828(2)	0.88(2)	0.0044(2)	0.00167(6)	0.0041(2)	0.00099(8)	0.0010(2)	0.00016(9)
Odm	0.1922(1)	0.86780(8)	0.4172(2)	0.89(2)	0.0042(2)	0.00148(6)	0.0045(2)	−0.00022(8)	0.0007(2)	−0.00012(9)

TABLE 3. Intensity collection and refinement results for reedmergnerite as a function of pressure

P (GPa)		0.00(5)	0.88(5)	1.89(5)	3.00(7)	3.64(7)	4.68(9)
No. obs $I > 2\sigma$		475	457	468	436	445	413
p^{**}		0.045	0.043	0.050	0.045	0.043	0.032
R_w		0.054	0.049	0.060	0.051	0.051	0.042
Unweighted *R*		0.044	0.040	0.050	0.041	0.043	0.041
GOF		1.17	1.13	1.19	1.13	1.16	1.16
Na	*x*	0.2587(5)	0.2572(4)	0.2560(5)	0.2544(5)	0.2541(5)	0.2534(5)
	y	0.0076(2)	0.0080(2)	0.0082(2)	0.0088(2)	0.0090(2)	0.0096(2)
	z	0.134(1)	0.132(1)	0.131(1)	0.129(1)	0.130(1)	0.128(1)
	B_{eq}	1.4(3)	1.7(3)	1.7(3)	1.8(3)	1.8(3)	1.6(3)
	β_{11}	0.005(1)	0.006(1)	0.006(1)	0.007(1)	0.007(1)	0.006(1)
	β_{22}	0.0034(1)	0.0031(1)	0.0029(2)	0.0028(1)	0.0030(1)	0.0025(1)
	β_{33}	0.007(6)	0.013(6)	0.015(7)	0.017(6)	0.016(6)	0.015(6)
	β_{12}	0.0007(3)	0.0007(2)	0.0005(3)	0.0010(3)	0.0009(3)	0.0001(3)
	β_{13}	0.002(2)	0.004(2)	0.005(3)	0.006(3)	0.005(3)	0.005(3)
	β_{23}	−0.0010(5)	−0.0016(5)	−0.0021(7)	−0.0012(6)	−0.0013(5)	−0.0026(6)
B	*x*	0.013(1)	0.014(1)	0.012(1)	0.013(1)	0.012(1)	0.013(1)
	y	0.1611(4)	0.1606(3)	0.1596(4)	0.1589(4)	0.1581(4)	0.1566(4)
	z	0.222(3)	0.222(3)	0.219(3)	0.222(3)	0.220(3)	0.220(3)
	B(iso)	0.53(8)	0.65(8)	0.6(1)	0.58(8)	0.56(8)	0.55(9)
Si1m	*x*	0.0062(3)	0.0054(3)	0.0052(3)	0.0052(3)	0.0046(3)	0.0055(3)
	y	0.80987(9)	0.80987(9)	0.8100(1)	0.8101(1)	0.8101(1)	0.8098(1)
	z	0.2098(6)	0.2085(6)	0.2089(7)	0.2085(7)	0.2071(6)	0.2092(7)
	B(iso)	0.53(3)	0.60(3)	0.56(3)	0.56(3)	0.61(3)	0.57(3)
Si2o	*x*	0.7029(3)	0.7023(3)	0.7010(4)	0.6992(3)	0.6992(3)	0.6986(4)
	y	0.1020(1)	0.1011(1)	0.1002(1)	0.0990(1)	0.0986(1)	0.0979(1)
	z	0.3205(7)	0.3216(7)	0.3211(9)	0.3192(8)	0.3207(7)	0.3199(8)
	B(iso)	0.50(3)	0.55(3)	0.52(3)	0.53(3)	0.61(3)	0.51(3)
Si2m	*x*	0.6857(4)	0.6828(4)	0.6798(4)	0.6760(4)	0.6738(4)	0.6715(4)
	y	0.8646(1)	0.86399(9)	0.8633(1)	0.8624(1)	0.8618(1)	0.8611(1)
	z	0.3566(8)	0.3551(8)	0.355(1)	0.3539(8)	0.3529(8)	0.3517(9)
	B(iso)	0.49(3)	0.49(3)	0.49(3)	0.54(3)	0.61(3)	0.52(3)
Oa1	*x*	0.0070(7)	0.0060(7)	0.0075(9)	0.0080(8)	0.0053(7)	0.0063(8)
	y	0.1370(3)	0.1362(2)	0.1350(3)	0.1350(3)	0.1340(3)	0.1333(3)
	z	0.002(2)	0.001(2)	0.003(2)	0.004(2)	1.000(2)	0.003(2)
	B(iso)	0.84(6)	0.87(6)	0.79(7)	0.87(6)	0.83(6)	0.83(7)
Oa2	*x*	0.5927(7)	0.5894(6)	0.5833(7)	0.5816(7)	0.5785(7)	0.5748(7)
	y	0.9811(2)	0.9806(2)	0.9794(3)	0.9800(2)	0.9788(3)	0.9783(3)
	z	0.275(1)	0.276(1)	0.270(2)	0.275(1)	0.272(2)	0.269(2)
	B(iso)	0.60(6)	0.65(5)	0.51(6)	0.51(6)	0.71(6)	0.62(6)
Obo	*x*	0.8448(7)	0.8456(7)	0.8458(8)	0.8482(8)	0.8486(7)	0.8484(8)
	y	0.0991(3)	0.0960(2)	0.0926(3)	0.0898(3)	0.0877(3)	0.0855(3)
	z	0.212(2)	0.213(2)	0.212(2)	0.216(2)	0.217(2)	0.216(2)
	B(iso)	0.85(6)	0.81(5)	0.77(7)	0.78(6)	0.87(6)	0.78(6)
Obm	*x*	0.8159(8)	0.8148(7)	0.8117(8)	0.8103(8)	0.8111(7)	0.8093(8)
	y	0.8346(3)	0.8351(2)	0.8345(3)	0.8335(3)	0.8334(3)	0.8325(3)
	z	0.232(2)	0.234(1)	0.231(2)	0.229(2)	0.233(2)	0.230(2)
	B(iso)	0.96(6)	1.01(6)	0.92(7)	0.95(6)	0.92(6)	0.91(7)
Oco	*x*	0.0062(7)	0.0033(7)	−0.0010(8)	−0.0056(7)	−0.0075(7)	−0.0116(7)
	y	0.2769(2)	0.2756(2)	0.2741(3)	0.2728(2)	0.2722(2)	0.2714(3)
	z	0.273(1)	0.272(1)	0.271(2)	0.270(2)	0.272(2)	0.270(2)
	B(iso)	0.64(6)	0.68(5)	0.73(7)	0.65(6)	0.70(6)	0.69(7)
Ocm	*x*	0.0295(7)	0.0288(7)	0.0275(8)	0.0268(8)	0.0269(8)	0.0265(8)
	y	0.6798(3)	0.6797(2)	0.6793(3)	0.6790(3)	0.6788(3)	0.6786(3)
	z	0.207(2)	0.204(2)	0.201(2)	0.200(2)	0.199(2)	0.194(2)
	B(iso)	0.76(6)	0.85(5)	0.81(7)	0.91(6)	0.97(6)	0.80(6)
Odo	*x*	0.190(1)	0.193(1)	0.195(1)	0.198(1)	0.2002(9)	0.202(1)
	y	0.1187(3)	0.1195(3)	0.1202(3)	0.1211(3)	0.1216(3)	0.1223(3)
	z	0.383(2)	0.383(2)	0.383(2)	0.383(2)	0.384(2)	0.383(2)
	B(iso)	0.98(7)	1.06(7)	0.97(8)	1.02(7)	1.05(7)	0.92(8)
Odm	*x*	0.1907(9)	0.1904(8)	0.193(1)	0.195(1)	0.1950(9)	0.195(1)
	y	0.8676(3)	0.8677(3)	0.8686(4)	0.8689(3)	0.8690(3)	0.8691(3)
	z	0.415(2)	0.412(2)	0.415(2)	0.418(2)	0.415(2)	0.414(2)
	B(iso)	1.03(6)	1.12(6)	1.14(8)	1.12(7)	1.09(7)	1.04(7)

the parameters is provided in Table 3. The restricted access imposed by the diamond cell, as well as the orientation of the crystal, prevented refinement of anisotropic displacement factors for all atoms but Na. The data and refinement is similar in quality to those in the studies on low albite (Downs et al. 1994) and microcline (Allan and Angel 1997).

RESULTS

Equation of state and unit-cell strain

The weighted volume and pressure data (Table 1) were fit to a nonlinear third-order Birch-Murnahan equation of state that gave a zero pressure volume, $V_0 = 589.17(3)$ Å^3, a zero pressure bulk modulus, $K_0 = 71(2)$ GPa, and

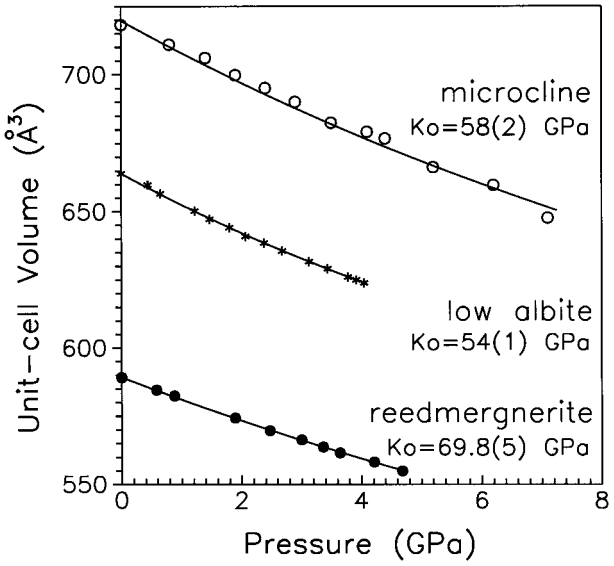

FIGURE 2. Unit-cell volumes of reedmergnerite, low albite, and microcline as a function of pressure. The symbols represent experimental data from Table 1 of this study (filled circles), Downs et al. (1994) (asterisks) and Allan and Angel (1997) (open circles) respectively. The lines represent weighted non-linear best-fit curves for third-order Birch-Murnahan equations of state.

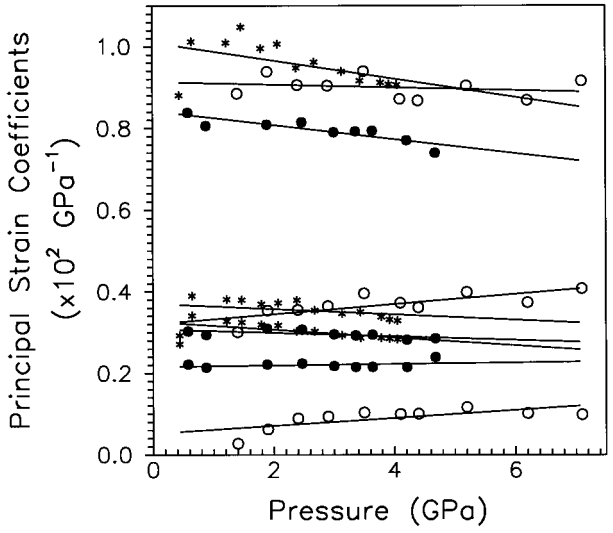

FIGURE 3. Principal strain coefficients as a function of pressure for reedmergnerite (filled circles), low albite (asterisks), and microcline (open circles). See Figure 2 for references. This figure demonstrates that each structure has a direction that is quite compressible in comparison to the orthogonal directions.

its pressure derivative, $K_0' = 3.3(12)$. Inasmuch as the pressure derivative is poorly defined, the fitting was repeated with $K_0' \equiv 4.0$, resulting in the same V_0 and a zero pressure bulk modulus, $K_0 = 69.8(5)$ GPa. This value agrees well with the value of 68.7(7) GPa reported by Hackwell and Angel (1992). The volume compressibility curve obtained in the constrained fit (Fig. 2) along with the data recorded for our crystal are compared to the data and curves for microcline and low albite. Albite is the most compressible of these minerals, followed by microcline and then reedmergnerite.

The principal coefficients for unit strain ellipsoids were computed between the cell parameters obtained at room pressure and those obtained at pressure using the Strain computer program of Ohashi (Hazen and Finger 1982) and are plotted in Figure 3 for all three structures. Each structure is quite compressible along one direction, but less than half as compressible in the orthogonal directions. The strain ellipsoids (Fig. 4) demonstrate that the most compressible direction for each mineral is that which narrows the channels containing the alkali cations. Each mineral compresses by different mechanisms as discussed below.

T-O bond and T-O-T angle compression

Selected bond lengths and angles computed for reedmergnerite are listed in Table 4. As with the other alkali feldspars, the T-O bond lengths do not seem to compress much, if at all, upon application of modest pressure, consistent with a model of rigid tetrahedra.

All Na-O bond lengths decrease smoothly with the application of pressure (Fig. 5). The compressibility of each bond is simply a function of the orientation of the bond with respect to the strain ellipsoid. The Na-Oa2 bond decreases the most with pressure because it is oriented more-or-less along the longest axis of the ellipsoid, which is perpendicular to the orientation of the chains. The Na-Obo and Na-Odo bond lengths decrease the least with

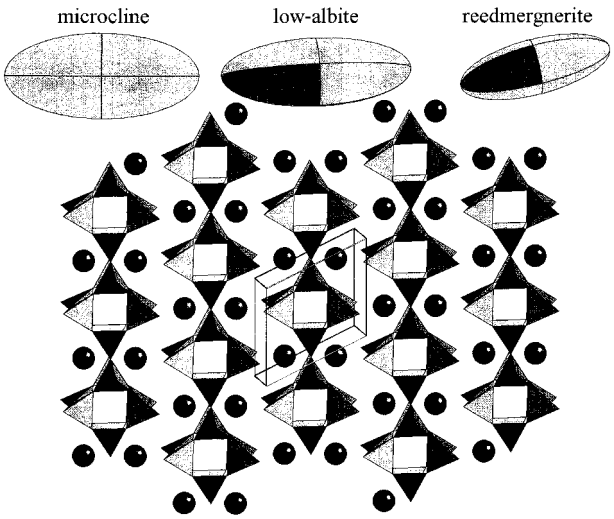

FIGURE 4. A slice ($0.2 < y < 0.8$) of the crystal structure of reedmergnerite viewed down b^*. The bottom layer of this slice is the top layer in Figure 1. Imposed above the crystal structure drawing are the strain ellipsoids for reedmergnerite, low-albite and microcline in the same orientation as the crystal structure. This figure illustrates the crystallographic controls on the directions of compression.

TABLE 4. Selected bond lengths and angles for reedmergnerite as a function of pressure

P (GPa)	0.00	0.00(5)	0.88(5)	1.89(5)	3.00(7)	3.64(7)	4.68(9)	$\partial_x/\partial P^*$
⟨T1o-O⟩	1.471(1)	1.475(6)	1.474(6)	1.468(7)	1.463(7)	1.470(7)	1.462(7)	−0.002(1)
⟨T1m-O⟩	1.6116(5)	1.603(4)	1.599(3)	1.604(4)	1.605(4)	1.598(4)	1.596(4)	−0.002(1)
⟨T2o-O⟩	1.6158(5)	1.618(3)	1.620(3)	1.620(4)	1.608(4)	1.612(4)	1.614(4)	−0.001(1)
⟨T2m-O⟩	1.6200(5)	1.622(3)	1.617(3)	1.618(4)	1.620(3)	1.613(3)	1.619(4)	−0.001(1)
Na-Oa1	2.454(1)	2.466(5)	2.442(5)	2.403(6)	2.375(5)	2.372(6)	2.341(6)	−0.026(2)
Na-Oa1	2.492(1)	2.495(5)	2.468(5)	2.445(6)	2.428(5)	2.399(5)	2.388(5)	−0.023(1)
Na-Oa2	2.404(1)	2.399(6)	2.370(5)	2.324(6)	2.302(5)	2.277(6)	2.248(6)	−0.033(1)
Na-Obo	2.401(1)	2.413(9)	2.384(9)	2.348(13)	2.340(12)	2.338(11)	2.307(12)	−0.021(2)
Na-Odo	2.375(1)	2.371(8)	2.366(8)	2.350(9)	2.336(9)	2.319(8)	2.309(9)	−0.014(1)
⟨Na-O⟩	2.4253(5)	2.428(3)	2.406(3)	2.374(4)	2.357(4)	2.341(3)	2.318(4)	−0.023(1)
T1o-Oa1-T1m	143.00(8)	143.7(3)	143.3(3)	142.6(4)	143.2(3)	142.4(3)	142.6(4)	−0.18(8)
T2o-Oa2-T2m	128.89(6)	128.4(4)	127.9(3)	126.2(4)	127.0(4)	126.3(4)	125.5(4)	−0.63(12)
T1o-Obo-T2o	139.57(9)	140.0(6)	138.6(6)	137.1(7)	136.2(7)	135.4(6)	134.6(6)	−1.13(6)
T1m-Obm-T2m	158.11(8)	157.0(7)	158.3(6)	157.0(7)	156.9(7)	159.2(7)	157.6(7)	0.07(21)
T1o-Oco-T2m	124.98(8)	124.5(3)	123.8(3)	123.1(4)	121.8(3)	121.3(3)	119.9(4)	−1.00(5)
T1m-Ocm-T2o	135.58(7)	135.8(4)	135.9(4)	135.6(5)	136.0(5)	136.2(5)	135.4(5)	0.01(7)
T1o-Odo-T2m	134.73(9)	135.1(6)	135.2(6)	135.9(7)	135.4(7)	135.6(7)	135.8(8)	0.17(6)
T1m-Odm-T2o	146.38(7)	146.4(4)	146.2(3)	146.1(4)	146.6(4)	146.1(4)	145.7(4)	−0.09(6)
⟨T-O-T⟩	138.90	138.86	138.65	137.95	137.89	137.81	137.14	−0.35(4)

* *x* refers to the particular bond length or the bond angle considered.

pressure because they are oriented more-or-less along the least compressible directions. It is unlikely that the M-O bonds directly influence compressibilities in the alkali feldspars because the bonds are so weak as to be rather incidental when compared to the other bonding constraints imposed by the T-O-T angles. The average M-O bond length varies with pressure as −0.023(1), −0.031(2), and −0.021(1) Å /GPa for reedmergnerite, low-albite, and microcline, respectively.

There are various compression trends for the T-O-T angles, with the angles associated with Obo and Oco decreasing significantly compared to the other angles (Fig. 6). In this respect reedmergnerite is similar to low-albite and quite different from microcline wherein the Al-Obo-Si and Si-Obm-Si angles undergo significant compression compared to the others. The variety of trends is essentially consistent with Baur's (1995) conclusion and Allan and Angel's (1997) observation that the feldspars are effectively non-collapsible framework structures, where changes in volume can be associated with changes in individual T-O-T angles, but the overall average angle does not vary. We find that <T-O-T> changes with pressure as −0.35(4), −0.23(6), and −0.39(4) °/GPa for reedmergnerite, low-albite, and microcline, respectively. In comparison, the Si-O-Si angle in quartz varies as −1.4(1)

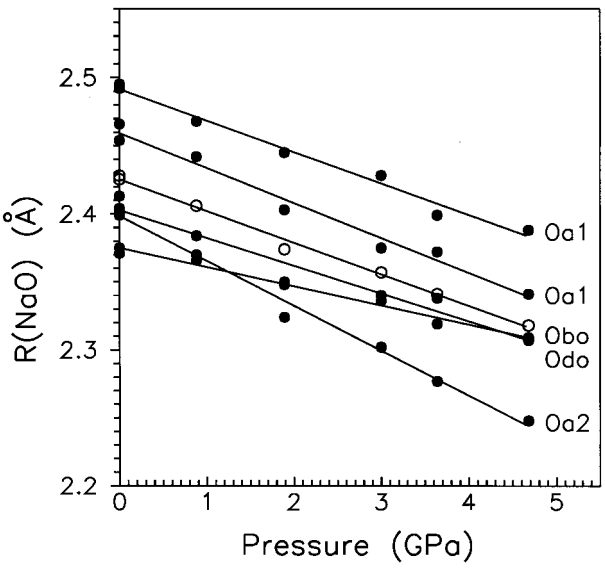

FIGURE 5. Na-O bond length as a function of pressure for reedmergnerite. The average Na-O bond length is symbolized with open circles. Errors are roughly the size of the symbols.

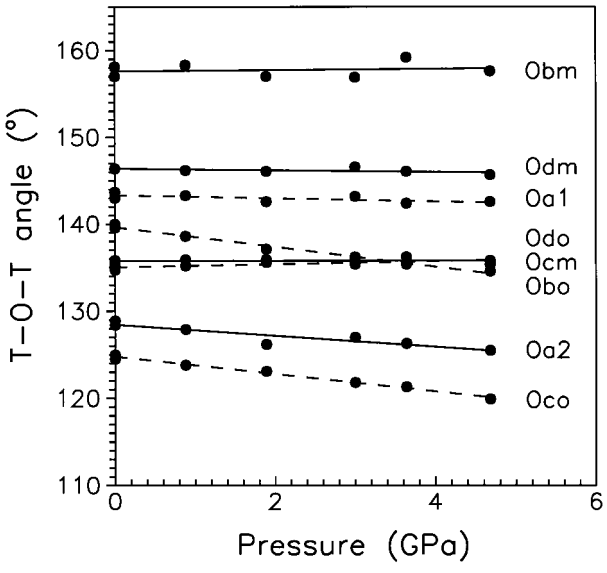

FIGURE 6. Variation of T-O-T angles with pressure for reedmergnerite. Regressed fits to the B-O-Si data are indicated with dashed lines whereas those associated with Si-O-Si are indicated with solid lines.

°/GPa (Glinnemann et al. 1992), −5.7(2) °/GPa in cristobalite (Downs and Palmer 1994) and −0.58(2) °/GPa in coesite (Levien and Prewitt 1981). The comparison with coesite is especially enlightening because its bulk modulus is about 100 GPa, quite large compared to the alkali feldspars, and yet the overall angle bending is significantly greater for coesite than for the alkali feldspars.

Comparison with albite

In spite of the differences between the B-O-Si and Al-O-Si angle bending energetics, the individual T-O-T angles associated with common O atoms in both albite and reedmergnerite follow very similar responses to compression. By this we mean that the angles associated with Oco and Obo decrease significantly in both structures, the angle associated with Obm remains relatively unchanged, and so on. The initial values of the angles differ, as expected because B-O-Si and Al-O-Si have different equilibrium values, but all the trends are similar. Thus, the two structures compress with similar mechanisms, and the differences in bulk moduli can be accounted for by the differences in T-O-T angle energetics. As in albite (Fig. 1), reedmergnerite also compresses by a mechanism that slides the chains of four-membered rings over each other. Analysis of pro-crystal electron density maps generated for reedmergnerite, computed as in the Downs et al. (1996) study, show that Na is bonded to the same 5 O atoms as occurs in albite. Thus, the similarity in compression mechanism for both structures results from similarities in Na-O bonding.

Comparison with microcline

The electron density study by Downs et al. (1996) demonstrated that the K atom in microcline is sevenfold coordinated. In particular, the K atom is bonded to all bridging O atoms involved with Al-O-Si linkages, including Oco, the atom that is not bonded to Na in albite or reedmergnerite. Interestingly, the Al-Oco-Si angle in microcline bends less than any of the other angles, whereas it bends the most in albite and reedmergnerite. Instead, Obo and Obm bend the most (Allan and Angel 1997). The net effect is to shear the four-membered rings (Fig. 1). The K-Obo distance is the longest for any of the O atoms that are bonded to Al, so the Al-Obo-Si angle should have the smallest bending force constant in the structure. Downs et al. (1996) also showed that Obm was not bonded to K, which would make it one of the weakest Si-O-Si angles. Thus, compression mechanisms in feldspars can be correlated with bending force constants of T-O-T linkages, which in turn are constrained by M-O bonding.

We now consider the apparent change in compression mechanism observed at ~4 GPa in microcline by Allan and Angel (1997). Such a change could occur if the bonding around the K atom were also to change upon application of pressure. Therefore, the pro-crystal electron density was computed for the reported microcline structures at pressure in the same manner as Downs et al. (1996). Below 4 GPa there is no (3,−1) critical point in the electron density that can be associated with K and Obm, but above 4 GPa such a critical point appears (Fig. 7). According to Bader (1990), a (3,−1) critical point located on the bond path between a pair of atoms means that the pair of atoms are bonded. It would seem that changing the bonding of the K atom would change the bending energetics of all associated T-O-T linkages, which would then change the compression mechanism of the structure. An examination of the bending of the Si-Obm-Si angle shows that it has a distinct change in slope with pressure. Below 4.4 GPa the angle changes −1.8 / GPa, whereas above 4.4 GPa it changes −3.5 /GPa. This change can be interpreted as follows. With application of

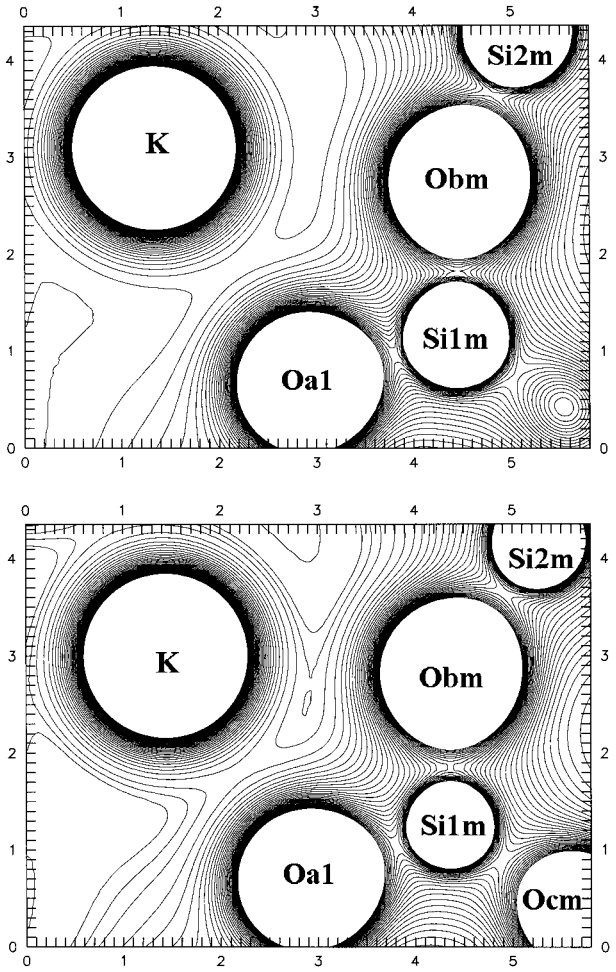

FIGURE 7. Pro-crystal electron density maps for microcline constructed at ambient conditions (top) and at P = 7.1 GPa (bottom) using the structures reported by Allan and Angel (1997). The maps are from a section of the structure constrained to the plane that include K, Obm, and Oal. At ambient conditions (top) there is no critical point in the electron density between K and Obm, but at 7.1 GPa (bottom) such a critical point exists. This signifies that a bond exists between K and Obm at high but not low pressure. The bonding changes can account for observed changes in compression mechanism.

pressure the four-membered rings shear in such a way that Obm is thrust out into the channels and consequently into the bonding region of the K atom. A bond is subsequently formed and upon further application of pressure both the Obm and K atoms are drawn even closer together. This explains the reported displacement of the K atom and the change in Si-Obm-Si slope. It is unclear as to how suddenly the bond appears. Bader (1990) believes that bond formation is practically instantaneous. However, in this case the data available for microcline are not sufficiently close spaced to make a judgement.

In summary, T-O-T angle bending appears to control the compression of these structures, but the constraints imposed on the energetics of angle bending are strongly dependent upon chemistry of the tetrahedral cations and upon the bonding of extra-framework cations. The tetrahedral cations can effect significant changes in bulk modulus, whereas the extra-framework cations also affect compression mechanism.

Acknowledgments

Support from the National Science Foundation (grant no. EAR-9218845) and the Carnegie Institution of Washington is gratefully acknowledged. Reviews by Ross Angel and Joe Smyth and editorial input by Anne Hofmeister greatly improved the manuscript, and we thank them.

References cited

Allan, D.R. and Angel, R.J. (1997) A high-pressure structural study of microcline ($KAlSi_3O_8$) to 7 GPa. European Journal of Mineralogy, 9, 263–275.

Angel, R.J. (1994) Feldspars at high pressure. In I. Parsons, Ed., Feldspars and their reactions, NATO ASI series C, Mathematical and Physical Sciences, p. 271–312. Kluwer Academic, Dordrecht, The Netherlands.

Angel, R.J., Allan, D.R., Miletich, R., and Finger, L.W. (1997) the use of quartz as an internal pressure standard in high-pressure crystallography. Journal of Applied Crystallography, 30, 461–466.

Appleman, D.E. and Clark, J.R. (1965) Crystal structure of reedmergnerite, a boron albite, and its relation to feldspar crystal chemistry. American Mineralogist, 50, 1827–1850.

Bader, R.F.W. (1990) Atoms in Molecules, A Quantum Theory. The International Series of Monographs in Chemistry 22. Clarendon Press, Oxford. 438 p.

Becker, P.J. and Coppens, P. (1975) Extinction within the limits of validity of the Darwin transfer equations: III. Non-spherical crystals and anisotropy of extinction. Acta Crystallographica, A31, 417–425.

Bridgman, P.W. (1923) The compressibility of thirty metals as a function of temperature and pressure. Proceedings of the American Academy of Arts and Science, 58, 165–242.

Downs, R.T. and Palmer, D.C. (1994) The pressure behavior of cristobalite. American Mineralogist, 79, 9–14.

Downs, R.T., Hazen, R.M., and Finger, L.W. (1994) The high-pressure crystal chemistry of low albite and the origin of the pressure dependency of Al-Si ordering. American Mineralogist, 79, 1042–1052.

Downs, R.T., Andalman, A., and Hudacsko, M. (1996) The coordination numbers of Na and K atoms in low albite and microcline as determined from a procrystal electron-density distribution. American Mineralogist, 81, 1344–1349.

Doyle, P.A. and Turner, P.S. (1968) Relativistic Hartree-Fock X-ray and electron scattering factors. Acta Crystallographica, A24, 390–397.

Finger, L.W. and Prince, E. (1975) A system of FORTRAN IV computer programs for crystal structure computations, 128 p. U.S. National Bureau of Standards, Technical Note 854.

Fleet, M.E. (1992) Tetrahedral-site occupancies in reedmergnerite and synthetic boron albite ($NaBSi_3O_8$). American Mineralogist, 77, 76–84.

Geisinger, K.L., Gibbs, G.V., and Navrotsky, A. (1985) A molecular orbital study of bond length and angle variations in framework structures. Physics and Chemistry of Minerals, 11, 266–283.

Glinnemann, J., King, H.E. Jr., Schulz, H., Hahn, T., La Placa, S.J., and Dacol, F. (1992) Crystal structures of the low-temperature quartz-type phases of SiO_2 and GeO_2 at elevated pressure. Zeitschrift f≈r Kristallographie, 198, 177–212.

Hackwell, T.P. and Angel, R.J. (1992) The comparative compressibility of reedmergnerite, danburite and their aluminum analogues. European Journal of Mineralogy, 4, 1221–1227.

Hazen, R.M. and Finger, L.W. (1982) Comparative Crystal Chemistry, 231 p. Wiley, New York.

Hemley, R.J., Prewitt, C.T., and Kingma, K.J. (1994) High-pressure behavior of silica. In Silica: Physical Behavior, Geochemistry and Materials Applications, P.J. Heaney, C.T. Prewitt and G.V. Gibbs, Editors, Reviews in Mineralogy, 29, Mineralogical Society of America, Washington, D.C.

Ibers, J.A. and Hamilton, W.C., Eds. (1974) International Tables for X-ray Crystallography, Vol IV, 366 p. Kynoch, Birmingham, U.K.

King, H.E. and Finger, L.W. (1979) Diffracted beam crystal centering and its application to high-pressure crystallography. Journal of Applied Crystallography, 12, 374–378.

Levien, L. and Prewitt, C.T. (1981) High-pressure crystal structure and compressibility of coesite. American Mineralogist, 66, 324–333.

Mao, H.K., Bell, P.M., Shaner, J.W., and Steinberg, D.J. (1978) Specific volume measurements of Cu, Mo, Pd, and Ag and calibration of the ruby R_1 fluorescence pressure gauge from 0.06 to 1 Mbar. The Journal of Applied Physics, 49, 3276–3283.

Merrill, L. and Bassett, W.A. (1974) Miniature diamond anvil pressure cell for single crystal X-ray diffraction studies. Review of Scientific Instruments, 45, 290–294.

Milton, C., Chao, E.C.T., Axelrod, J.M., and Grimaldi, F.S. (1960) Reedmergnerite, $NaBSi_3O_8$, the boron analogue of albite, from the Green River Formation, Utah. American Mineralogist, 45, 188–199.

Milton, C., Axelrod, J.M., and Grimaldi, F.S. (1954) New minerals, reedmergnerite, ($Na_2O{\bullet}B_2O_3{\bullet}6SiO_2$) and eitelite ($Na_2O{\bullet}MgO_2CO_2$), associated with leucosphenite, shortite, searlesite, and crocidolite in the Green River formation, Utah. Geological Society of America Bulletin, 65, 1286–1287.

Nicholas, J.B., Winans, R.E., Harrison, R.J., Iton, L.E., Curtiss, L.A., and Hopfinger, A.J. (1992) Ab initio molecular orbital study of the effects of basis set size on the calculated structure and acidity of hydroxyl groups in framework molecular sieves. The Journal of Physical Chemistry, 96, 10247–10257.

Manuscript received May 21, 1998
Manuscript accepted October 8, 1998
Paper handled by John Parise